Journal of Solid State Chemistry 184 (2011) 953–958

Contents lists available at ScienceDirect

Journal of Solid State Chemistry

journal homepage: www.elsevier.com/locate/jssc

Rapid Communication

Preparation of magnetic $CoFe_2O_4$-functionalized graphene sheets via a facile hydrothermal method and their adsorption properties

Nianwu Li [a], Mingbo Zheng [b], Xiaofeng Chang [a], Guangbin Ji [a], Hongling Lu [a], Luping Xue [a], Lijia Pan [b], Jieming Cao [a,*]

[a] Nanomaterials Research Institute, College of Materials Science and Technology, Nanjing University of Aeronautics and Astronautics, Nanjing 210016, China
[b] National Laboratory of Microstructures, School of Electronic Science and Engineering, Nanjing University, Nanjing 210093, China

ARTICLE INFO

Article history:
Received 9 October 2010
Received in revised form
28 December 2010
Accepted 16 January 2011
Available online 25 January 2011

Keywords:
$CoFe_2O_4$
Magnetic
Graphene
Nanocomposites
Adsorption

ABSTRACT

Magnetic $CoFe_2O_4$-functionalized graphene sheets ($CoFe_2O_4$–FGS) nanocomposites have been synthesized by hydrothermal treatment of inorganic salts and thermal exfoliated graphene sheets. Scanning electron microscopy (SEM) and transmission electron microscopy (TEM) observations show that cobalt ferrite nanoparticles with sizes of 10–40 nm are well dispersed on graphene sheets. OH^- was recognized as a tie to integrate the inorganic salts with the graphene sheets, which made reaction started and developed on the surface of graphene sheets and formed cobalt ferrite nanoparticles on graphene sheets. The adsorption kinetics investigation revealed that the adsorption of methyl orange from aqueous solution over the as-prepared $CoFe_2O_4$–FGS nanocomposites followed pseudo-second-order kinetic model and the adsorption capacity was examined as high as 71.54 mg g^{-1}. The combination of the superior adsorption of FGS and the magnetic properties of $CoFe_2O_4$ nanoparticles can be used as a powerful separation tool to deal with water pollution.

1. Introduction

Magnetic nanoparticles and carbon nanotubes nanocomposites have applications in waste water treatment and drug delivery [1–3]. Graphene, a two-dimensional honeycomb lattice formed by a flat monolayer of hexagonally arrayed sp^2-bonded carbon atoms, is the basal building block in all graphitic materials [4,5]. It has excellent mechanical [6], electrical [7], thermal [8], optical properties [9], high surface area (calculated value, 2630 m^2 g^{-1}) [10], and fascinating transport phenomena (such as the quantum hall effect) [11]. It is believed that magnetic nanoparticles and graphene nanocomposites would have better performances in these applications.

Recently only a few researchers have managed to fabricate magnetic graphene nanocomposites [12–15]. Yang's group prepared GO (graphene oxide) and Fe_3O_4 nanoparticles nanocomposites via the chemical precipitation method under N_2 atmosphere, and showed their application in drug carriers [12]. Yu's group prepared magnetite (Fe_3O_4) nanoparticles functionalized RGO (reduced graphene oxide) using $Fe(acac)_3$ as precursor and refluxing at 278 °C under an argon protection, and showed its potential application in magnetic resonance image [13]. Fan and co-workers attached Fe_3O_4 nanoparticles to graphene oxide by covalent bonding [14]. Magnetite and RGO nanocomposites also have been reported for an arsenic removal [15]. Up to now, all the magnetic graphene nanocomposites are carried out on GO and RGO.

As another main graphene derivate to prepare graphene nanocomposites, FGS (functionalized graphene sheets) have the highest BET surface area (300–900 m^2 g^{-1}), and a broad pore size distribution in the range 2–200 nm stacked by graphene sheets [16,17], thus it is a potential excellent adsorption material. Consequently, it is considered as a novel adsorbent, which has great potential in the treatment of contaminant from an aqueous solution. To the best of our knowledge, the preparation and adsorption properties of $CoFe_2O_4$–FGS nanocomposites have not been reported.

Herein, we report a facile hydrothermal method to prepare $CoFe_2O_4$–FGS nanocomposites. On the basis of results obtained from microstructure characterization, the cobalt ferrite nanoparticles with diameters of 10–40 nm were uniformly distributed on FGS and the formation mechanism of $CoFe_2O_4$ nanoparticles on graphene sheets was initially discussed. To investigate the adsorption of $CoFe_2O_4$–FGS, the usual contaminant methyl orange (MO) was selected as the model compound. Furthermore, we demonstrated that $CoFe_2O_4$–FGS nanocomposites have great potential as an effective absorbent for removing MO in water, due to its high adsorption capacity and convenient magnetic separation.

* Corresponding author. Fax: +86 25 84895289.
E-mail address: jmcao@nuaa.edu.cn (J. Cao).

0022-4596/$ - see front matter © 2011 Published by Elsevier Inc.
doi:10.1016/j.jssc.2011.01.014

2. Experimental

2.1. Preparation of FGS

GO was prepared from natural graphite powders by hummer's method [18]. FGS were prepared according to our previous report [17]. GO was put into quartz tube preheated to 300 °C and held in the quartz tube for 3 min. These thermal exfoliated graphene sheets were signed as FGS.

2.2. Preparation of $CoFe_2O_4$–FGS

To investigate the microstructures of the proposed nanocomposites effectively, typical $CoFe_2O_4$–FGS composites with the selected mass ratio of 1:2 were prepared according to the following description. For the preparation of $CoFe_2O_4$–FGS nanocomposites, FGS (50 mg) were added to 50 ml distilled water. $Co(AC)_2 \cdot 4H_2O$ and $FeCl_3 \cdot 6H_2O$ with a mole ratio of 1:2 were added to the suspension. The solution was stirred for 12 h. Then, 0.5 M NaOH was added to the suspension until the pH=12. The solution was stirred for 10 min and supersonic vibrated for 2 min, followed by a hydrothermal treatment at 150 °C for 24 h under static conditions. The black product was washed in distilled water for several times, and then collected by vacuum filtration. The final product was obtained after drying at 60 °C under vacuum. The sample was signed as $CoFe_2O_4$–FGS. Additionally, for the magnetic measurement, the $CoFe_2O_4$–FGS samples with mass ratios of 1:1 and 1:4 were selected and prepared as well according to similar route mentioned above.

2.3. Characterization and magnetic property

X-ray powder diffraction (XRD) analysis was performed on X-ray diffractometer (Bruker D8 ADVANCE). X-ray photoelectron spectroscopy (XPS) was measured by Kratos Ultra DLD spectrometer. Fourier transform infrared spectroscopy (FTIR) was tested on Nicolet-670 spectrophotometer. Field-emission scanning electron microscopy (SEM) images were obtained on LEO 1530 Gemini scanning gun electron microscope. Transmission electron microscopy (TEM, including high-resolution TEM, HR-TEM) images and selective area electron diffraction (SAED) patterns were recorded by using JEOL JEM-2100 transmission electron microscope. The magnetic properties of nanocomposites were studied by vibrating sample magnetometer (VSM, lakeshore, Model 7404). The N_2 adsorption–desorption analysis was measured on the Micromeritics ASAP 2010 instrument.

2.4. Adsorption experiment

$CoFe_2O_4$–FGS (mass ratio of 1:4) was selected as an adsorbent in the kinetics study, and the concentration of MO was 10 ppm, and the temperature was 30 °C. UV–vis spectrophotometer (VARIAN Cary 100) was employed to monitor the absorbance value of the MO solution by testing the wavelength at 464 nm, and the concentrations of the solutions were determined by using linear regression equation obtained by plotting a calibration curve for an MO over the concentration range 0–15 ppm. The removed quantity of an MO by the sample was calculated by the expression as follows:

$$q_t = \frac{(C_0 - C_t)V}{m} \quad (1.1)$$

where q_t represents the adsorption capacity at time t, C_0 (mg l^{-1}) is the initial methyl orange concentration, C_t (mg l^{-1}) is the equilibrium concentration of dye remaining in the solution at time t, V (l) is the volume of the aqueous solution, and m is the weight of powder sample.

3. Results and discussion

3.1. Characterization of $CoFe_2O_4$–FGS

The XRD pattern of the as-prepared $CoFe_2O_4$–FGS depicted in Fig. 1 shows diffraction peaks at 2θ=30.1°, 35.4°, 43.1°, 57.0°, 62.6°, which correspond to crystal indexes of (220), (311), (400), (511), and (440), respectively. All of the diffraction peaks can be indexed to the cubic spinel structure of cobalt ferrite (JCPDS no. 22-1086).

XPS measurement was used to study the surface components and the elements valences of the $CoFe_2O_4$–FGS. The C 1s, O 1s, Co 2p, Fe 2p core photoionization signals and O KLL, Fe LMM Auger signals are clearly displayed in the wide spectrum (Fig. 2a). In detail, the peak at the binding energy of 284.5 eV is related to the honeycomb carbon ring in the graphene sheets [19]. To assess the oxidation states of cobalt and iron on the surface of the $CoFe_2O_4$ nanocrystals, the Co 2p and Fe 2p spectra were investigated, as shown in Fig. 2b and c. From the Co 2p spectrum, it was found that the first two peaks with binding energies of about 780.6 and 786.6 eV correspond to Co $2p_{3/2}$ and its shake-up satellites, while the higher binding energies peaks around 795.5 and 802.6 eV were attributed to Co $2p_{1/2}$ and its shake-up satellites, respectively. The intense Co $2p_{3/2}$ shake-up satellite illustrated the presence of a large number of Co^{2+} species in the sample, because the low spin Co^{3+} cation only gave rise to much weaker satellite features than high spin Co^{2+} with unpaired valence 3d electron orbitals [20]. In addition, two peaks of an Fe 2p level with binding energies of 711.0 and 725.1 eV were assigned to Fe $2p_{3/2}$ and Fe $2p_{1/2}$, respectively. This result clearly demonstrated the presence of Fe^{3+} [21]. All the above analysis further confirmed the presence of $CoFe_2O_4$ nanocrystals on the surface of graphene sheets without any impurities.

The functionalized groups on GO, FGS, and $CoFe_2O_4$–FGS have been examined by FTIR, which is shown in Fig. 3. The absorption peak at 3423 cm^{-1} is due to the presence of –OH stretching modes. The peaks at 1727, 1569, 1405, 1232, and 1050 cm^{-1} can be assigned to the C=O, aromatic C=C, carboxy C–O, epoxy C–O, and C–O groups on the surface of graphene sheets, respectively. The strong peaks show that GO have high quality. When the GO decomposes into FGS, carboxy C–O, and C–O groups disappear, and other groups decrease obviously on the graphene sheets. Compared with FGS, the intensity of the peak at 3423 cm^{-1} for

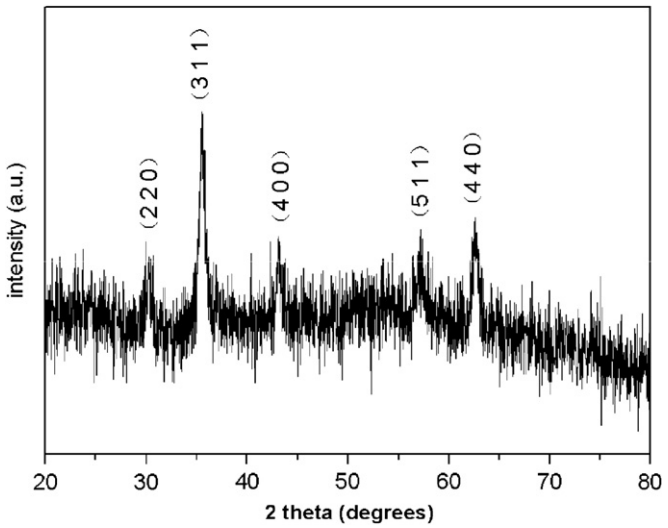

Fig. 1. XRD pattern of $CoFe_2O_4$–FGS.

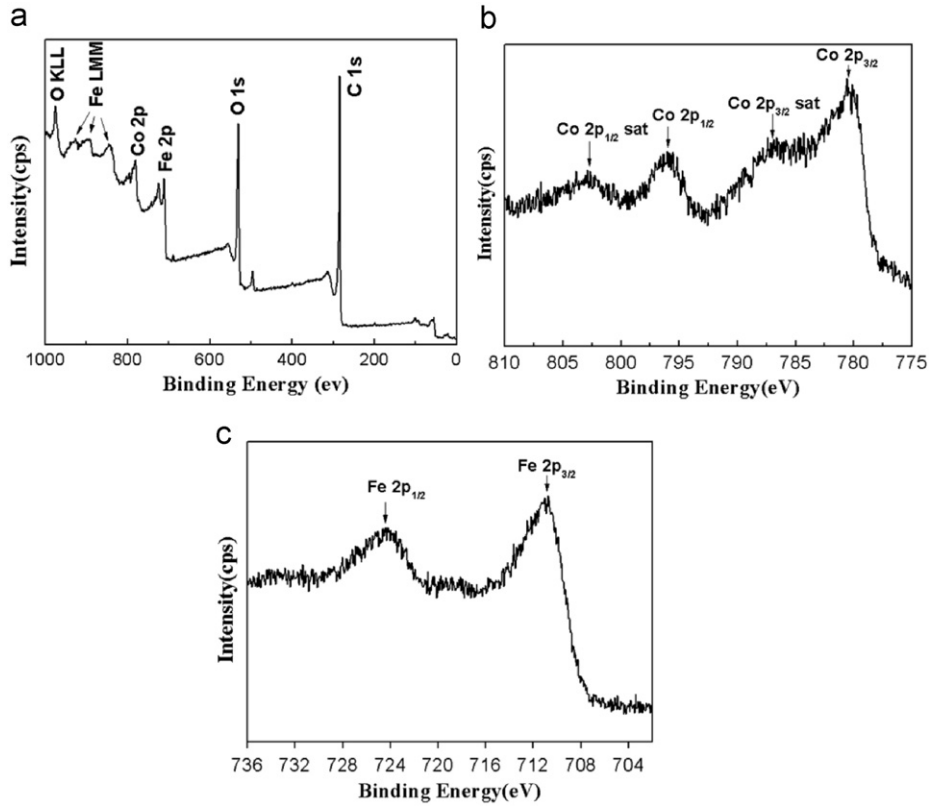

Fig. 2. Wide (a) and deconvoluted (b, c) XPS spectra of the as-prepared $CoFe_2O_4$–FGS.

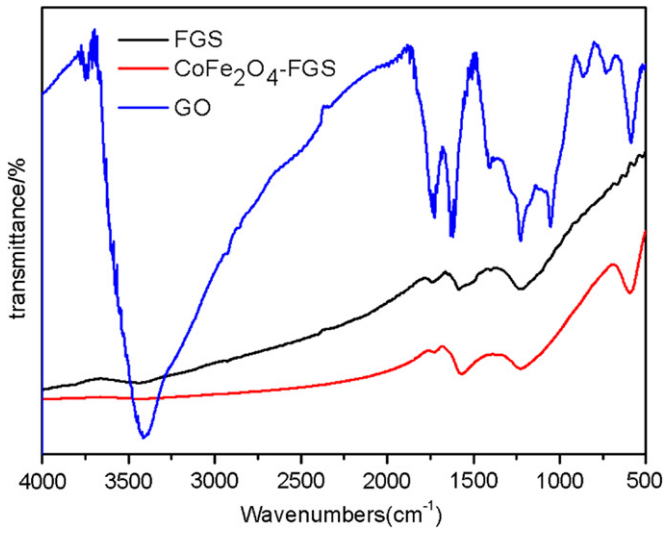

Fig. 3. FT-IR spectra of GO, FGS, and $CoFe_2O_4$–FGS.

$CoFe_2O_4$–FGS sample decreases, and a new sharp peak at 594 cm^{-1} is observed. According to the previous report, the stretching vibration peak gradually shifts from Fe–O bands in the 631 cm^{-1} to Fe(Co)–O bands in the 588 cm^{-1} with increasing of cobalt content in the cobalt ferrite [22]. The new sharp peak observed at 594 cm^{-1} also suggests that the new phase cobalt ferrite is formed by replacement of an Fe^{3+} by Co^{2+} as well, which enters the lattice of as-prepared products.

The SEM and TEM images of FGS (Fig. 4a, b) display a wrinkled paper-like structure of the ultrathin graphene sheets and stacking of sheets. Fig. 4c and d shows that $CoFe_2O_4$ nanoparticles uniformly disperse on the surface of graphene sheets and between the layers of graphene sheets. The details of $CoFe_2O_4$–FGS have been further examined by HR-TEM. Fig. 4e shows that the size of $CoFe_2O_4$ particles ranges 10–40 nm, and the $CoFe_2O_4$ particles uniformly disperse on graphene sheets. The selected area electron diffraction (SAED) pattern indicates that these small $CoFe_2O_4$ particles are polycrystals. On the basis of the HR-TEM image (Fig. 4f), the planar space of lattice fringes is about 0.48 nm, corresponding to the (1 1 1) plane of spinel $CoFe_2O_4$.

3.2. Formation mechanism of $CoFe_2O_4$–FGS

In our early report [17], FGS have many oxygen functional groups, a high BET surface area, and a broad pore size distribution in the range 2–200 nm stacked by graphene sheets. Therefore, it is an excellent graphene derivative to prepare graphene nanocomposites. Previous report demonstrated that the partially oxygenated FGS can disperse readily in polar solvents, and the oxygen functional groups also allow for an enhanced interaction with polar matrices [23]. And it was found that FGS can be well dispersed in water as the interaction between OH^- and functional groups of FGS. In Geim's perspective [24], graphene as a giant flat molecule can absorb and desorb various atoms and molecules (for example, NO_2, NH_3, K, and OH), and can participate in chemical reactions as well. Schematic representation of the formation mechanism of $CoFe_2O_4$–FGS has been illustrated in Fig. 5. The Co^{2+}, Fe^{3+} inorganic salt has strong interaction with OH^- in the suspension, thus OH^- becomes the tie to connect the inorganic salt and FGS. In addition, graphene sheets absorb the intermediate product and the final product. Therefore, the reaction started and developed on the surface of graphene sheets containing oxygen functional groups. At the same time, Co^{2+}, Fe^{3+} inorganic salt, and OH^- continuously accumulated in the reaction places. During the

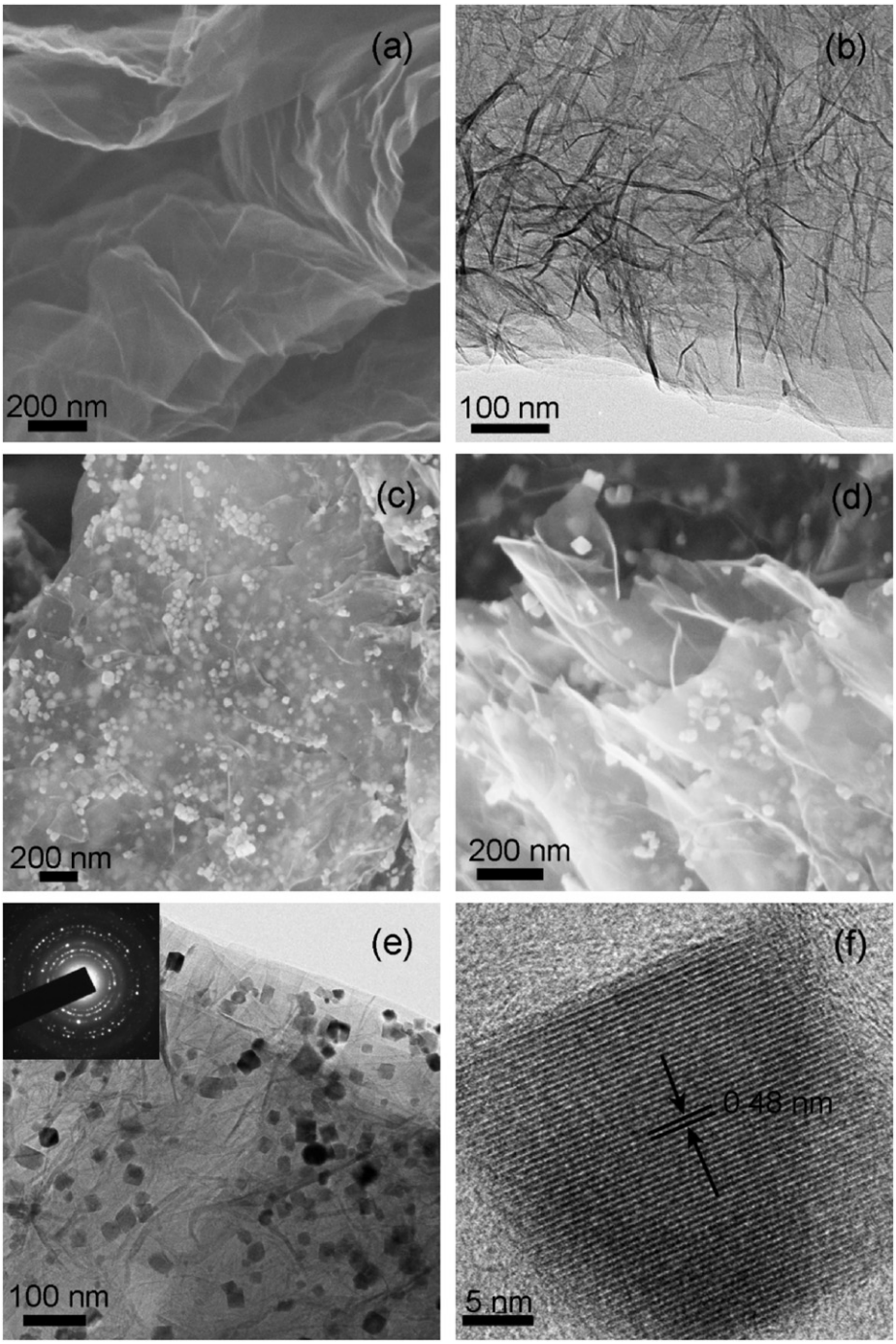

Fig. 4. SEM image of FGS (a); TEM image of FGS (b); SEM images of $CoFe_2O_4$–FGS (c, d); TEM image (e) and HR-TEM image (f) of $CoFe_2O_4$–FGS; the inset in (e) depicts the corresponding SAED pattern of $CoFe_2O_4$–FGS.

hydrothermal treating process, the $CoFe_2O_4$ nanoparticles were formed on the surface of graphene sheets.

3.3. Adsorption activity towards an MO

The magnetization curves of $CoFe_2O_4$–FGS tested at 300 K are depicted in Fig. 6. The hysteresis loops indicate that the ferromagnetic characteristics of as-prepared $CoFe_2O_4$–FGS nanocomposites and the coercivity of the nanocomposites are estimated at ~500 Oe, suggesting that such nanocomposites might be easily separated from solution phase through inducing an external magnetic field. The dependence of an MO removal % on sorption time between adsorbent and adsorbate, as depicted in Fig. 7a, shows that the adsorption–desorption equilibrium could be reached after the contact time of 60 min. In order to further calculate the relevant adsorption kinetic parameters, the obtained kinetic results were fitted by means of pseudo-second-order model, which can be expressed as follows [25]:

$$\frac{t}{q_t} = \frac{1}{k_2 q_e^2} + \frac{t}{q_e} = \frac{1}{v_0} + \frac{t}{q_e} \tag{1.2}$$

where k_2 is the rate constant of pseudo-second-order adsorption (min^{-1}); q_e and q_t are the amount of methyl orange adsorbed at equilibrium and at certain time t ($mg\,g^{-1}$); and v_0 ($mg\,g^{-1}\,min^{-1}$) is the initial sorption rate.

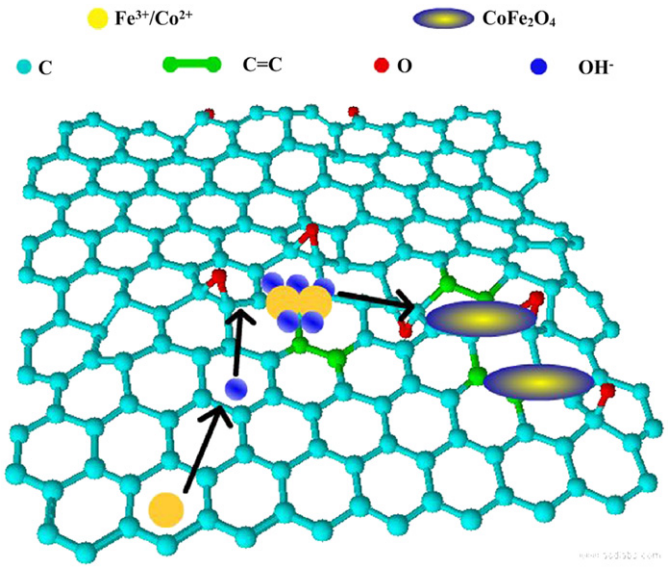

Fig. 5. Schematic illustration for the formation mechanism of $CoFe_2O_4$–FGS.

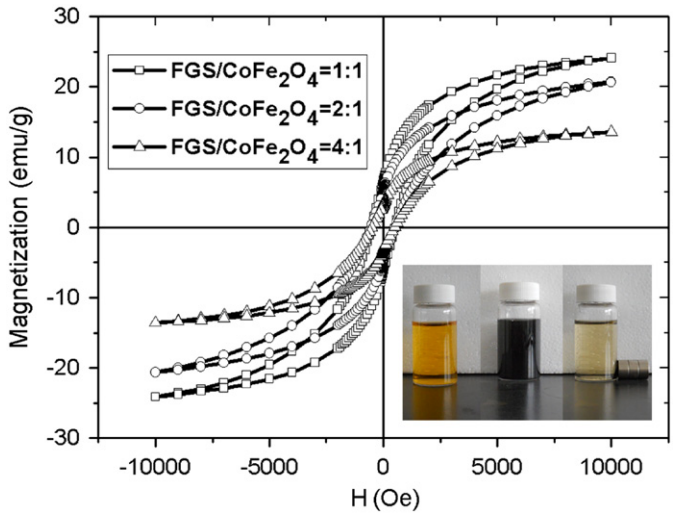

Fig. 6. Hysteresis loops of $CoFe_2O_4$–FGS with different $CoFe_2O_4$:FGS weight ratio of 1:1, 1:2, and 1:4 at 300 K. The inset picture shows the methyl orange solution, $CoFe_2O_4$–FGS dispersed in the dye solution, and magnetic separation.

As shown in Fig. 7a, the pseudo-second-order model fits all the sorption data well according to the high correlation coefficients ($r^2 > 0.97$). Thus, chemical interaction during the sorption process could be initially deduced. Fitting results by using intraparticle diffusion model [26] show that the adsorption process has good fitting linear relationship between q_t (adsorption capacity for a specific time) and $t^{0.5}$ (square root of the adsorption time) at the initial adsorption stage, but not passing through the origin point, implying that contribution of intraparticle diffusion is not the rate-controlling step. The initial pH value in the corresponding sorption process was measured at ~8. And no obvious change of pH value is found before and after the sorption. Fig. 8 depicts changes of adsorption capacity as a function of BET specific surface area for as-prepared $CoFe_2O_4$–FGS samples with different mass ratios. The increased adsorption capacity can be observed by increasing the mass ratio of FGS in the $CoFe_2O_4$–FGS. The highest adsorption capacity can be achieved at ~101.34 mg g^{-1} when selecting pure phase of FGS as the adsorbent, but such excellent adsorbent with high specific surface area of 330 m^2 g^{-1} cannot be separated from water easily. The magnetic separation experiment

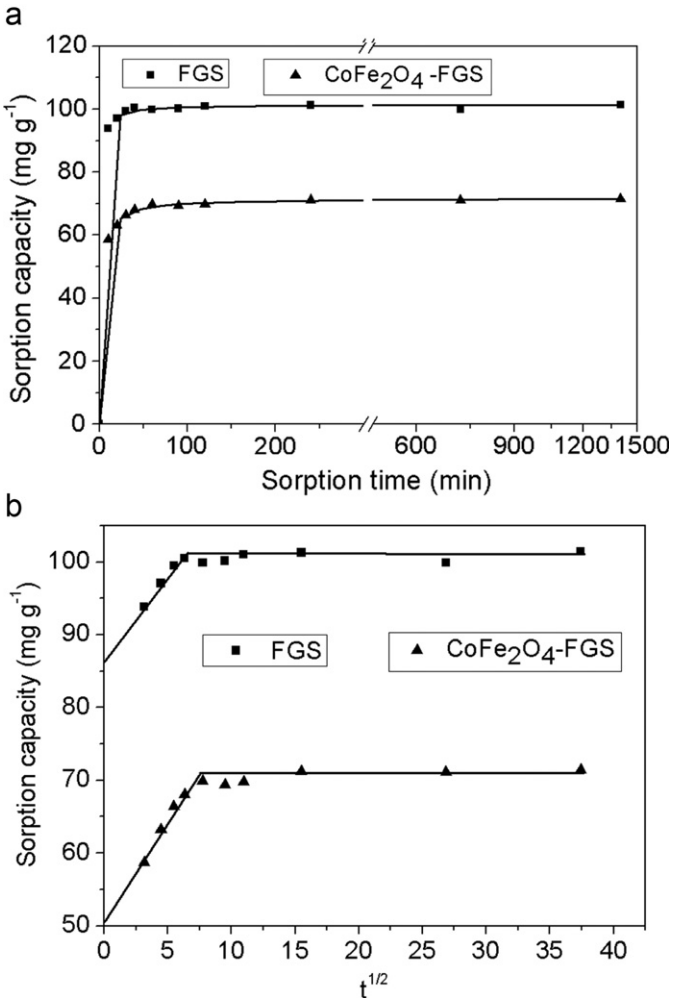

Fig. 7. Sorption kinetics of methyl orange on FGS and $CoFe_2O_4$–FGS modeling using the pseudo-second-order model (a) and the intraparticle diffusion model (b).

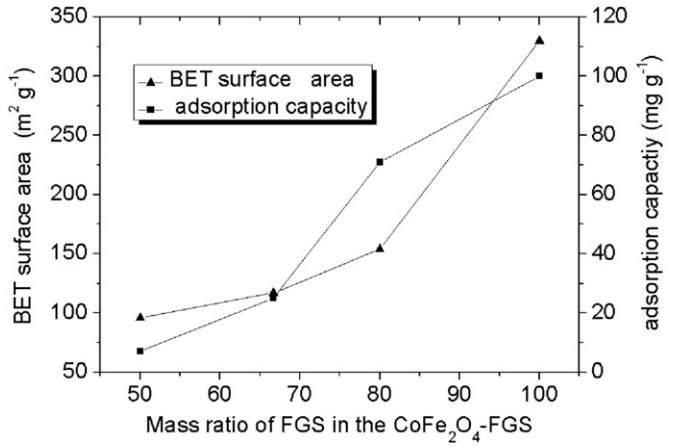

Fig. 8. The variation of adsorption capacity and BET surface area with increasing mass ratio of FGS in the $CoFe_2O_4$–FGS.

(inset of Fig. 6) obviously shows that the as-prepared $CoFe_2O_4$–FGS (mass ratio of 1:4) can be separated from the solution phase in several minutes by inducing an external magnetic field produced by Nd–Fe–B permanent magnet, though the initial sorption rate and adsorption capacity of an MO on the $CoFe_2O_4$–FGS decreases to 71.54 mg g^{-1}, compared to those of pure FGS

(101.34 mg g^{-1}), which was caused by the decreasing of the effective adsorption sites after combination of $CoFe_2O_4$ on FGS. However, it is worth noticing that adsorption capacity (71.54 mg g^{-1} at initial concentration of 10 ppm) of an MO over as-prepared $CoFe_2O_4$–FGS is much higher than that of newly developed adsorbent of m-CS/c-Fe_2O_3/MWCNTs (about 17 mg g^{-1} at identical operation conditions) [1], demonstrating the magnetic separable $CoFe_2O_4$–FGS is promising materials in fields of separation/purification-related technologies.

4. Conclusion

In the present study, magnetic $CoFe_2O_4$–FGS nanocomposites have been successfully synthesized via a facile hydrothermal approach. XRD, XPS, SEM, and TEM studies revealed the presence of high-crystalline cobalt ferrite phase on the surface of graphene sheets. It was demonstrated that the magnetic separable $CoFe_2O_4$–FGS has high adsorption capacity (71.54 mg g^{-1}) towards MO molecules with the initial concentration of 10 ppm. This study shows that the $CoFe_2O_4$–FGS could be beneficial for the separation/purification-related applications.

Acknowledgments

This work was supported by the Natural Science Foundation of Jiangsu Province (BK2006195 and BK2010497), National Natural Science Foundation of China (6076019 and 50701024), and NCET.

References

[1] H.Y. Zhu, R. Jiang, L. Xiao, G.M. Zeng, Bioresour. Technol. 101 (2010) 5063–5069.
[2] J.L. Gong, B. Wang, G.M. Zeng, C.P. Yang, C.G. Niu, Q.Y. Niu, W.J. Zhou, Y. Liang, J. Hazardous Mater. 164 (2009) 1517–1522.
[3] T.W. Lin, C.G. Salzmann, L.D. Shao, C.H. Yu, M.L.H. Green, S.C. Tsang, Carbon 47 (2009) 1415–1420.
[4] C.N.R. Rao, A.K. Sood, K.S. Subrahmanyam, A. Govindaraj, Angew. Chem. Int. Ed. 48 (2009) 7752–7777.
[5] M.J. Allen, V.C. Tung, R.B. Kaner, Chem. Rev. 110 (2010) 132–145.
[6] C. Lee, X.D. Wei, J.W. Kysar, J. Hone, Science 321 (2008) 385–388.
[7] K.I. Bolotin, K.J. Sikes, Z. Jiang, M. Klima, G. Fudenberg, J. Hong, P. Kim, H.L. Stormer, Solid State Commun. 146 (2008) 351–355.
[8] A.A. Balandin, S. Ghosh, W.Z. Bao, I. Calizo, D. Teweldebrhan, F. Miao, C.N. Lau, Nano Lett. 8 (2008) 902–907.
[9] F. Wang, Y.B. Zhang, C.S. Tian, C. Girit, A. Zettl, M. Crommie, Y.R. Shen, Science 320 (2008) 206–208.
[10] M.D. Stoller, S.J. Park, Y.W. Zhu, J.H. An, R.S. Ruoff, Nano Lett. 8 (2008) 3498–3502.
[11] Y.B. Zhang, Y.W. Tan, H.L. Stormer, P. Kim, Nature 438 (2005) 201–204.
[12] X.Y. Yang, X.Y. Zhang, Y.F. Ma, Y. Huang, Y.S. Wang, Y.S. Chen, J. Mater. Chem. 19 (2009) 2710–2714.
[13] H.P. Cong, J.J. He, Y. Lu, S.H. Yu, Small 6 (2010) 169–173.
[14] V. Chandra, J. Park, Y. Chun, J.W. Lee, I.C. Hwang, K.S. Kim, ACS Nano 4 (2010) 3979–3986.
[15] F. He, J.T. Fan, D. Ma, L.M. Zhang, C. Leung, H.L. Chan, Carbon 48 (2010) 3139–3144.
[16] M.J. McAllister, J.L. Li, D.H. Adamson, H.C. Schniepp, A.A. Abdala, J. Liu, M.H. Aloson, D.L. Milius, R. Car, R. k. Prud'homme, I.A. Aksay., Chem. Mater. 19 (2007) 4396–4404.
[17] Q.L. Du, M.B. Zheng, L.F. Zhang, Y.W. Wang, J.H. Chen, L.P. Xue, W.J. Dai, G.B. Ji, J.M. Cao, Electrochim. Acta 55 (2010) 3897–3903.
[18] W.S. Hummers, R.E. Offeman, J. Am. Chem. Soc. 20 (1958) 1339.
[19] S.Z. Zu, B.H. Han, J. Phys. Chem., C 113 (2009) 13651–13657.
[20] Z.J. Gu, X. Xiang, G.L. Fan, F. Li, J. Phys. Chem., C 112 (2008) 18459–18466.
[21] C. Altavilla, E. Ciliberto, A. Aiello, C. Sangergorio, D. Gatteschi, Chem. Mater. 19 (2007) 5980–5985.
[22] X. Fan, J.G. Guan, X.F. Cao, W. Wang, F.Z. Mou, Eur. J. Inorg. Chem. (2010) 419–426.
[23] T. Ramanatan, A.A. Abdala, S. Stankovich, D.A. Dikin, M. Herrera-alonso, R.D. Piner, D.H. Adamson, H.C. Schniepp, X. Chen, R.S. Ruoff, S.T. Nguyen, I.A. Aksay, R.K. Prud'homme, L.C. Brinson, Nat. Nanotechnol. 3 (2008) 327–330.
[24] A.K. Geim, Science 324 (2009) 1530–1534.
[25] Y.S. Ho, G. Mckay, Process Saf. Environ. 76 (1998) 332–340.
[26] X.Y. Yang, B. Al-Duri, J. Colloid Interface Sci. 287 (2005) 25–34.